Supplemental information

Potent monoclonal antibodies neutralize

Omicron sublineages and other SARS-CoV-2 variants

Zhaochun Chen, Peng Zhang, Yumiko Matsuoka, Yaroslav Tsybovsky, Kamille West, Celia Santos, Lisa F. Boyd, Hanh Nguyen, Anna Pomerenke, Tyler Stephens, Adam S. Olia, Baoshan Zhang, Valeria De Giorgi, Michael R. Holbrook, Robin Gross, Elena Postnikova, Nicole L. Garza, Reed F. Johnson, David H. Margulies, Peter D. Kwong, Harvey J. Alter, Ursula J. Buchholz, Paolo Lusso, and Patrizia Farci

Cell Reports

Supplemental Information

Potent monoclonal antibodies neutralize
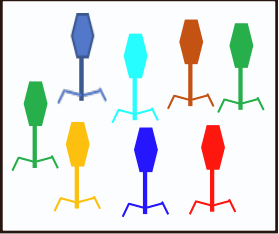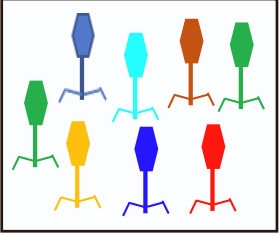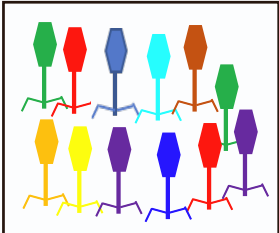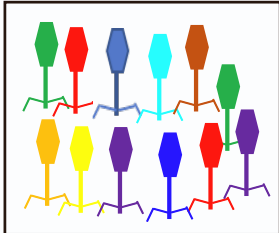
Omicron sublineages and other SARS-CoV-2 variants

Zhaochun Chen, Peng Zhang, Yumiko Matsuoka, Yaroslav Tsybovsky, Kamille West,

Celia Santos, Lisa F. Boyd, Hanh Nguyen, Anna Pomerenke, Tyler Stephens,

Adam S. Olia, Baoshan Zhang, Valeria De Giorgi, Michael R. Holbrook, Robin Gross,

Elena Postnikova, Nicole L. Garza, Reed F. Johnson, David H. Margulies,

Peter D. Kwong, Harvey J. Alter, Ursula J. Buchholz, Paolo Lusso, Patrizia Farci

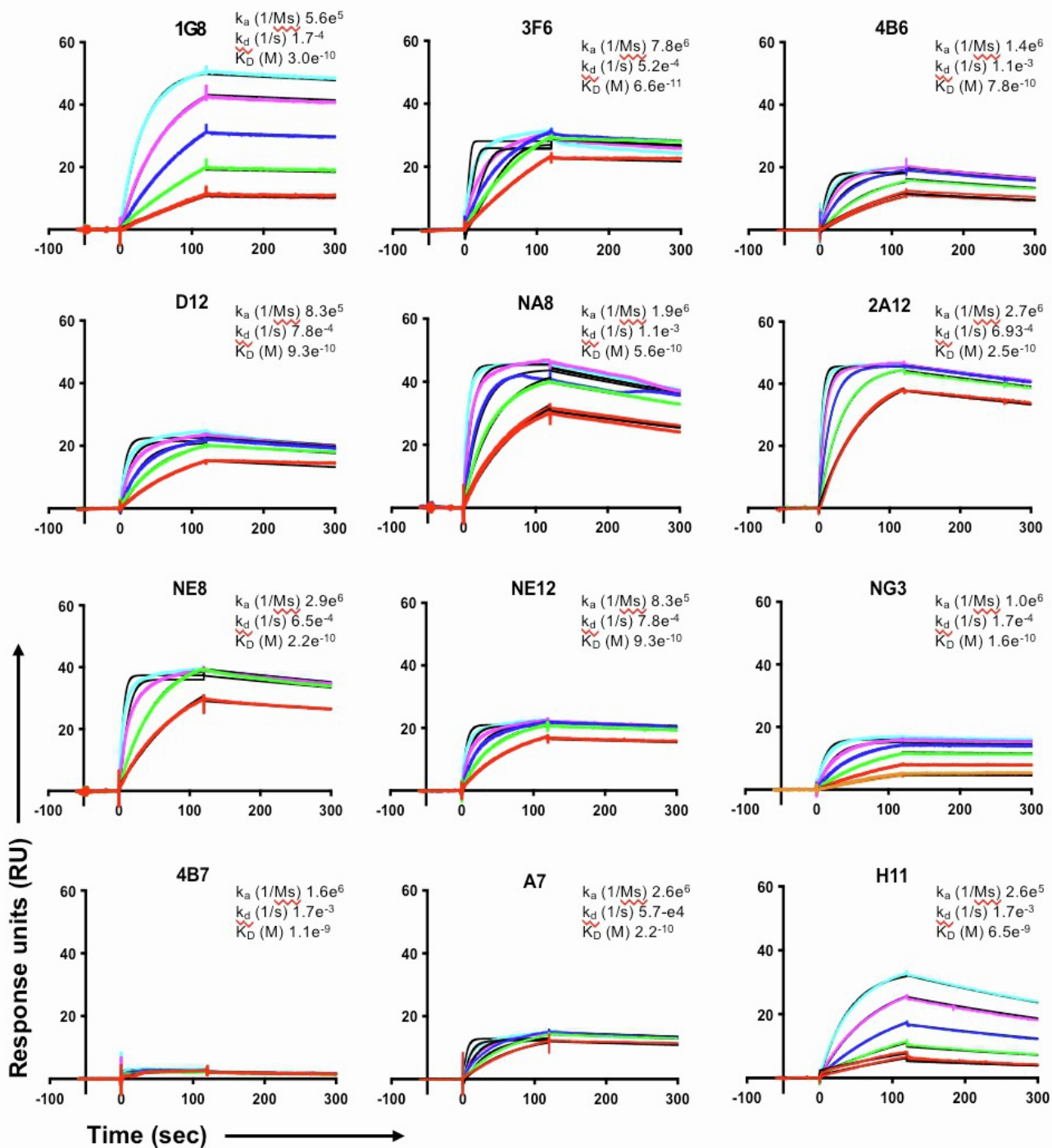| Single patient	Patient number	Neutralizing titer	Library size	Positive clones	Distinct clones
Library 1	1	80	4.2×10^7	12	1
Library 2	2	80	4.0×10^7	70	3

Multiple patients	Patient number	Neutralizing titer	Library size	Positive clones	Distinct clones
Library 3	3	80			
	4	80			
	5	320	9.1×10^8	300	9
	6	320			
	7	320			
Library 4	8	160			
	9	160			
	10	640	7.8×10^8	230	5
	11	160			
	12	640			

Figure S1. Characteristics of 4 phage-display Fab libraries, related to Figure 1. The libraries were generated from peripheral blood mononuclear cells (PBMC) obtained from convalescent COVID-19 donors, derived from either a single donor or five donors combined.

1G8

k_a (1/Ms) 5.6e^5
k_d (1/s) 1.7^{-4}
K_D (M) 3.0e^{-10}

3F6

k_a (1/Ms) 7.8e^6
k_d (1/s) 5.2e^{-4}
K_D (M) 6.6e^{-11}

4B6

k_a (1/Ms) 1.4e^6
k_d (1/s) 1.1e^{-3}
K_D (M) 7.8e^{-10}

D12

k_a (1/Ms) 8.3e^5
k_d (1/s) 7.8e^{-4}
K_D (M) 9.3e^{-10}

NA8

k_a (1/Ms) 1.9e^6
k_d (1/s) 1.1e^{-3}
K_D (M) 5.6e^{-10}

2A12

k_a (1/Ms) 2.7e^6
k_d (1/s) 6.93^{-4}
K_D (M) 2.5e^{-10}

NE8

k_a (1/Ms) 2.9e^6
k_d (1/s) 6.5e^{-4}
K_D (M) 2.2e^{-10}

NE12

k_a (1/Ms) 8.3e^5
k_d (1/s) 7.8e^{-4}
K_D (M) 9.3e^{-10}

NG3

k_a (1/Ms) 1.0e^6
k_d (1/s) 1.7e^{-4}
K_D (M) 1.6e^{-10}

4B7

k_a (1/Ms) 1.6e^6
k_d (1/s) 1.7e^{-3}
K_D (M) 1.1e^{-9}

A7

k_a (1/Ms) 2.6e^6
k_d (1/s) 5.7-e4
K_D (M) 2.2^{-10}

H11

k_a (1/Ms) 2.6e^5
k_d (1/s) 1.7e^{-3}
K_D (M) 6.5e^{-9}

Response units (RU)

Time (sec)

Figure S2. Binding profiles of 12 Fabs to a stabilized trimeric SARS-CoV-2 spike protein (S-2P), related to Figure 1. All the Fabs showed tight binding to the protein. The S-2P protein was coupled to the chip at a surface density 200-450 Rus. Fabs were flowed over the surface at graded concentrations ranging from 5.625 nM to 90 nM (color coded). Kinetic values were obtained using Biaeval 3.1; fits are indicated by the black lines.
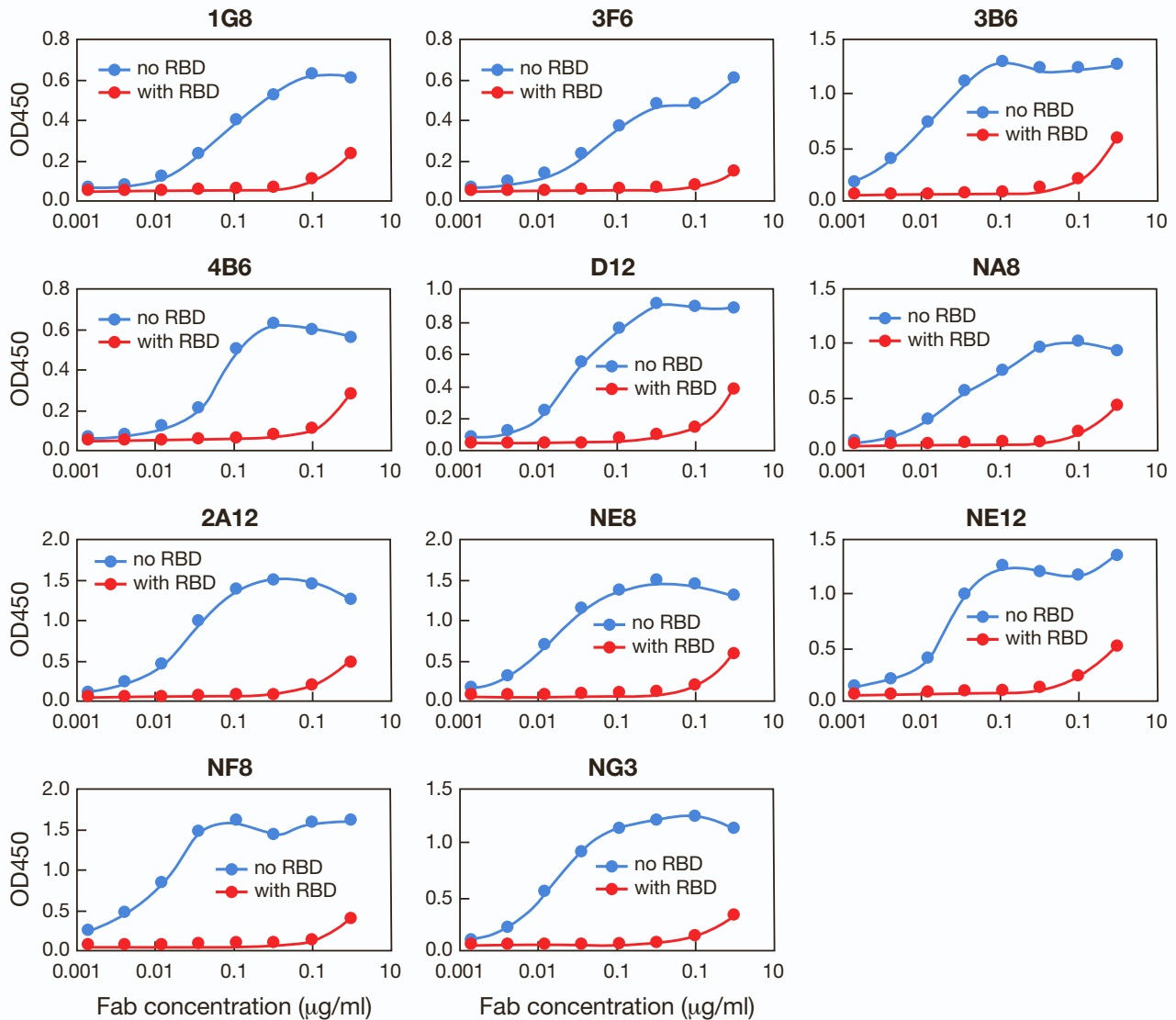
Figure S3. Binding of 12 Fabs derived from convalescent COVID-19 donors to the receptor-binding domain (RBD) of the SARS-CoV-2 spike protein, related to Figure 2. All of the Fabs shown, except one, are specific for the RBD, as demonstrated using the recombinant RBD protein as a competitor in ELISA. The red lines show the loss of signal when recombinant RBD was pre-incubated with the Fabs. Only one Fab, H11, was not inhibited, suggesting that its binding site is outside the RBD.

Fab →

IgG	NE12	NF8	NG3	1G8	3B6	3F6	4B6	D12	NA8	NE8	2A12
NE12	84	99	97	-31	90	30	58	58	62	85	82
NF8	78	99	67	-17	94	16	75	97	85	98	86
NG3	70	93	91	-64	93	57	98	84	72	82	75
1G8	41	73	45	92	72	92	84	86	82	87	42
3B6	55	87	61	-49	96	4	83	89	99	93	99
3F6	27	33	24	64	16	86	27	34	47	22	18
4B6	93	95	86	-38	98	5	80	87	81	97	78
D12	81	93	83	-30	95	6	74	80	61	86	87
NA8	69	88	65	-82	92	-18	37	63	51	74	76
NE8	46	78	41	-60	78	-19	18	47	42	61	61
2A12	68	88	70	-59	94	-15	28	66	64	84	86

Figure S4. Cross-competition of 11 monoclonal antibodies for binding to the SARS-CoV-2 spike protein (S-2P) trimer, related to Figure 2. To investigate if the epitopes recognized by the 11 monoclonal antibodies are distinct or overlapping, we performed cross-competition experiments between Fabs and complete IgG in ELISA. The percent competition was calculated using the following formula: [1- (average OD from wells containing test IgG with Fab – average OD from control wells)/(average OD from wells containing test IgG without Fab – average OD from control wells)] x100%.
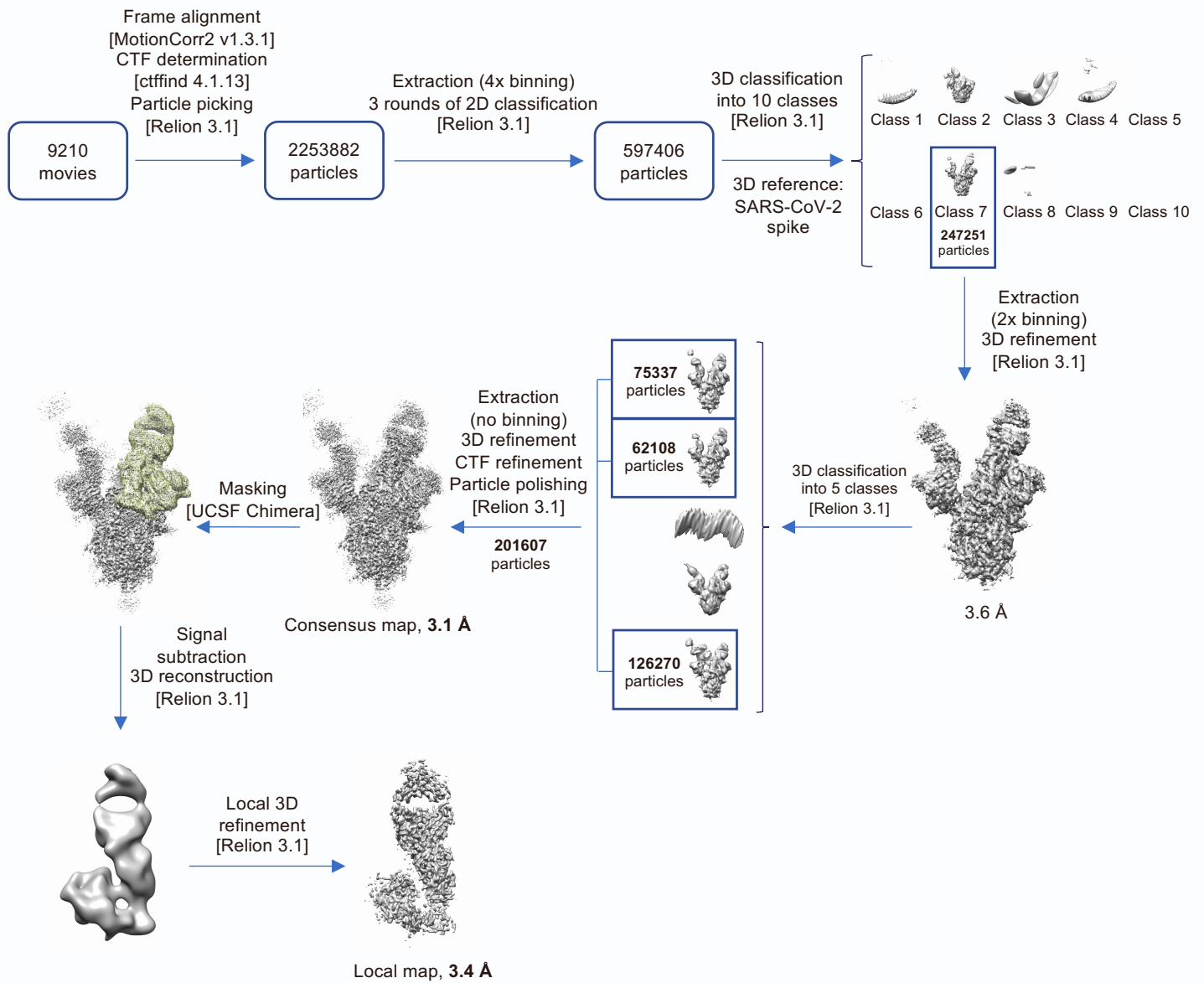
A

mAb	Live virus neutralization IC$_{50}$ (µg/ml)	
	WA-1	**B.1.351 Beta**
G6	>10	>10
4A12	>10	>10
4B7	>10	>10
A7	>10	>10
1B1	>10	>10
4C6	>10	>10
H11	>10	>10
1G8	3.969	0.298
3F6	3.150	0.221
3B6	0.020	>10
4B6	7.937	>10
D12	1.768	>10
NA8	0.442	0.039
2A12	0.039	>10
NE8	0.055	>10
NE12	0.028	>10
NF8	0.884	>10
NG3	0.055	>10
Lilly_CoV555	0.089	>10

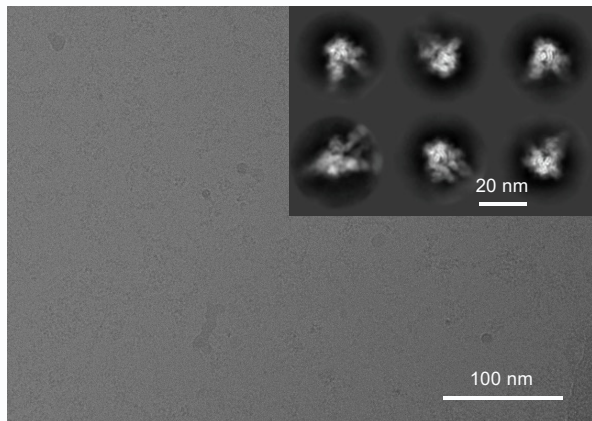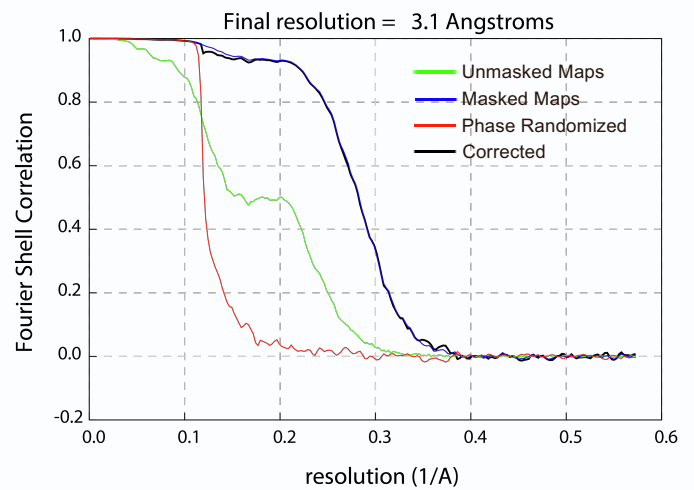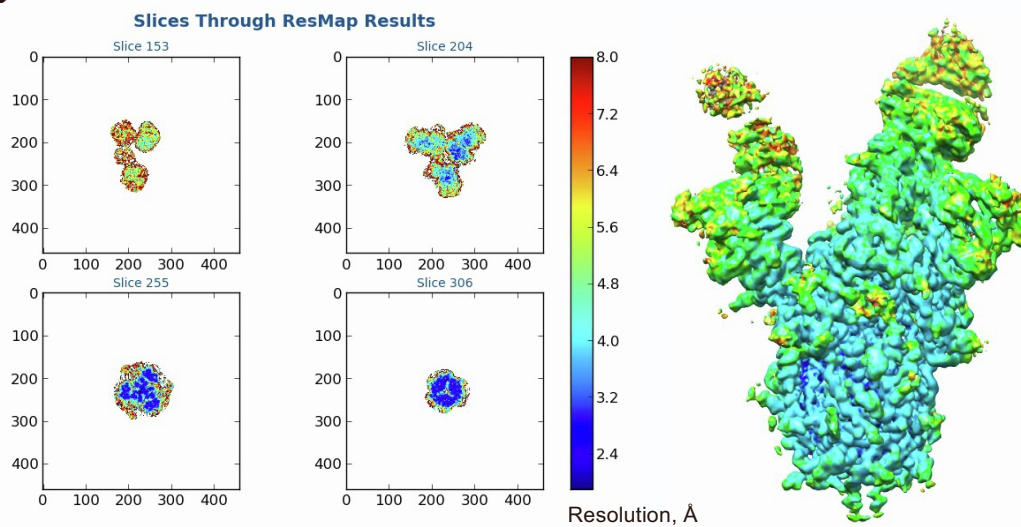| >10	10-1	1-0.1	0.1-0.01	<0.01

B

$R^2 = 0.8318$
$P < 0.0001$
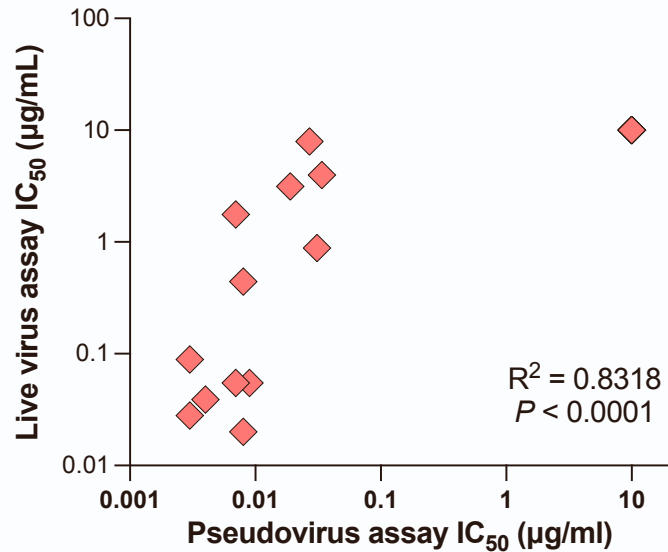
Figure S5. Live virus neutralization of WA-1 and B.1.351 SARS-CoV-2 strains by 18 monoclonal antibodies and correlation with pseudovirus neutralization, related to Figure 2. (A) Heat map of live virus neutralization against SARS-CoV-2 WA-1 and B.1.351. (B) Correlation between neutralizing activities of mAbs in the pseudovirus and live virus assays.

Frame alignment
[MotionCorr2 v1.3.1]
CTF determination
[ctffind 4.1.13]
Particle picking
[Relion 3.1]

9210 movies

Extraction (4x binning)
3 rounds of 2D classification
[Relion 3.1]

2253882 particles

3D classification
into 10 classes
[Relion 3.1]

3D reference:
SARS-CoV-2
spike

597406 particles

Class 1 Class 2 Class 3 Class 4 Class 5

Class 6 Class 7 Class 8 Class 9 Class 10
247251 particles

Extraction
(2x binning)
3D refinement
[Relion 3.1]

3.6 Å

3D classification
into 5 classes
[Relion 3.1]

75337 particles

62108 particles

126270 particles

Extraction
(no binning)
3D refinement
CTF refinement
Particle polishing
[Relion 3.1]

201607 particles

Consensus map, 3.1 Å

Masking
[UCSF Chimera]

Signal
subtraction
3D reconstruction
[Relion 3.1]

Local 3D
refinement
[Relion 3.1]

Local map, 3.4 Å

Figure S6. Cryo-EM data processing workflow leading to the structure of SARS-CoV-2 Spike in complex with Fab NE12, related to Figure 3. Software packages are indicated in square brackets.

A

20 nm

100 nm

B

Final resolution = 3.1 Angstroms

Fourier Shell Correlation

— Unmasked Maps
— Masked Maps
— Phase Randomized
— Corrected

resolution (1/A)

C

Slices Through ResMap Results

Slice 153

Slice 204

Slice 255

Slice 306

Resolution, Å

Figure S7. Validation of the consensus cryo-EM map of SARS-CoV-2 spike in complex with Fab NE12, related to Figure 3.
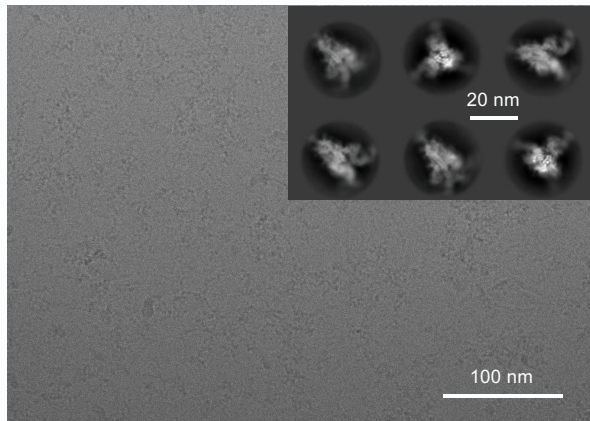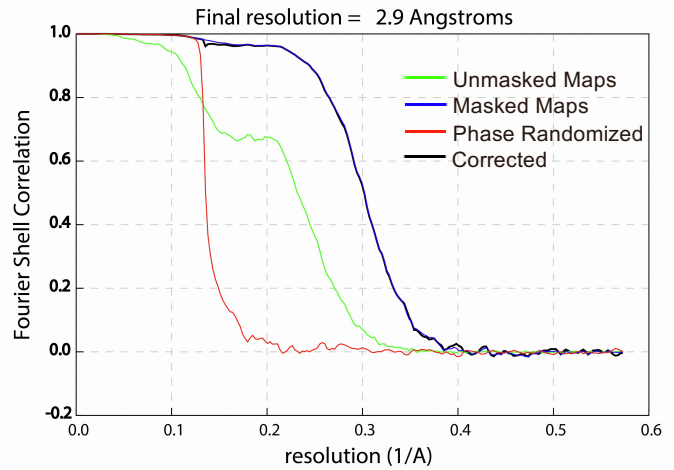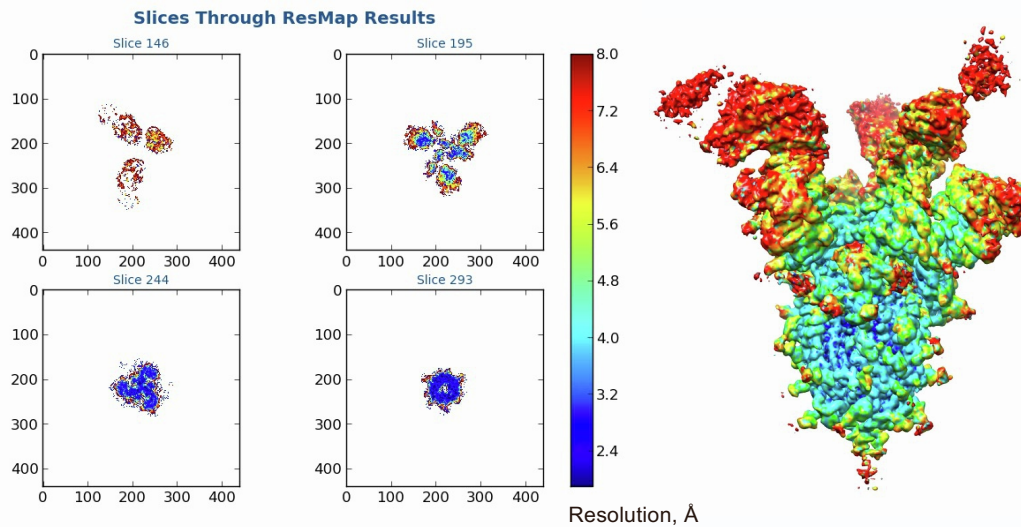
(A) Representative micrograph and 2D classes (insert).

(B) Fourier shell correlation (FSC) plots generated by Relion.

(C) Local resolution determined with ResMap.
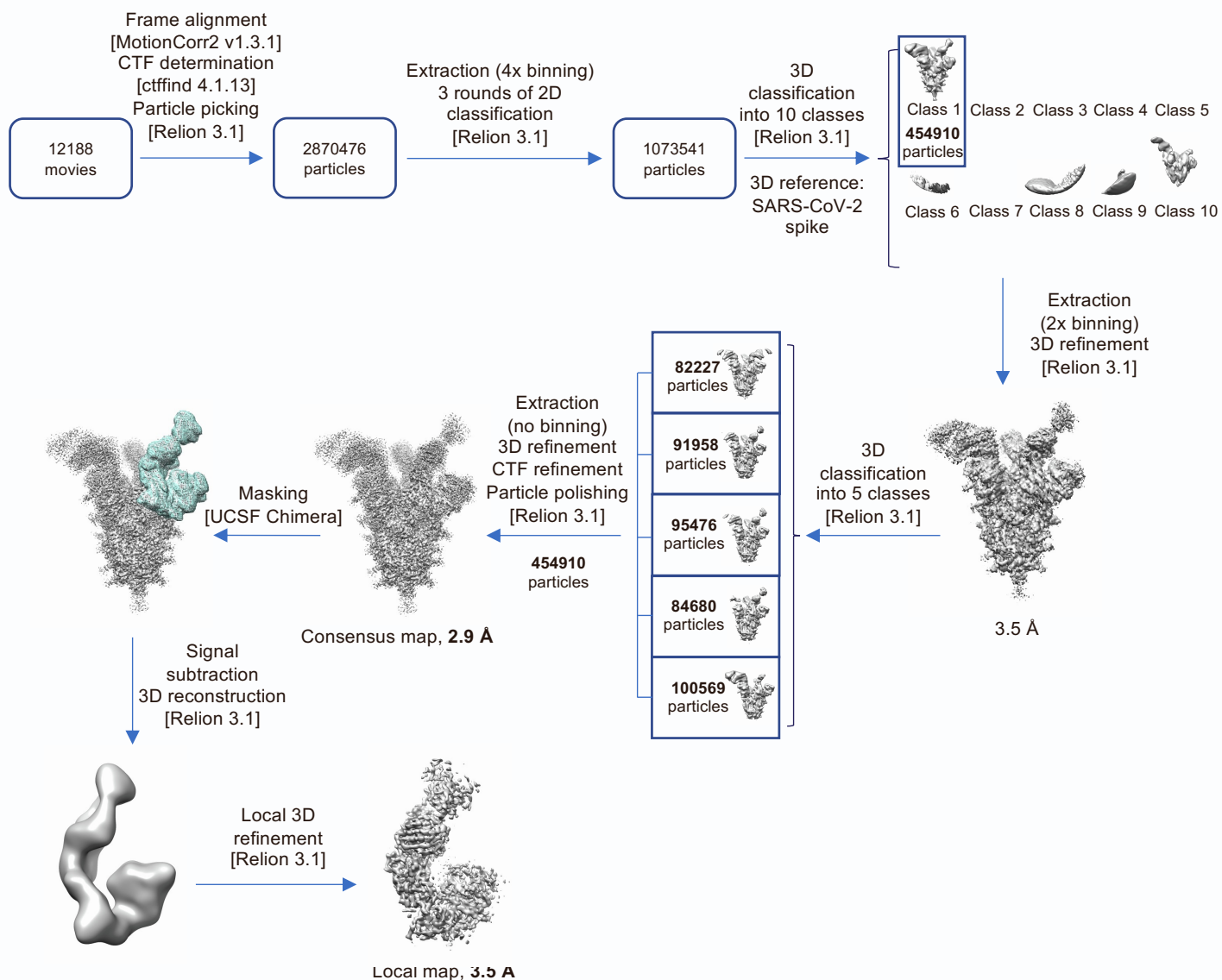
Figure S8. Cryo-EM data processing workflow leading to the structure of SARS-CoV-2 Spike in complex with Fab NA8, related to Figure 4. Software packages are indicated in square brackets.

Figure S9. Validation of the consensus cryo-EM map of SARS-CoV-2 spike in complex with Fab NA8, related to Figure 4.

(A) Representative micrograph and 2D classes (insert).

(B) Fourier shell correlation (FSC) plots generated by Relion.

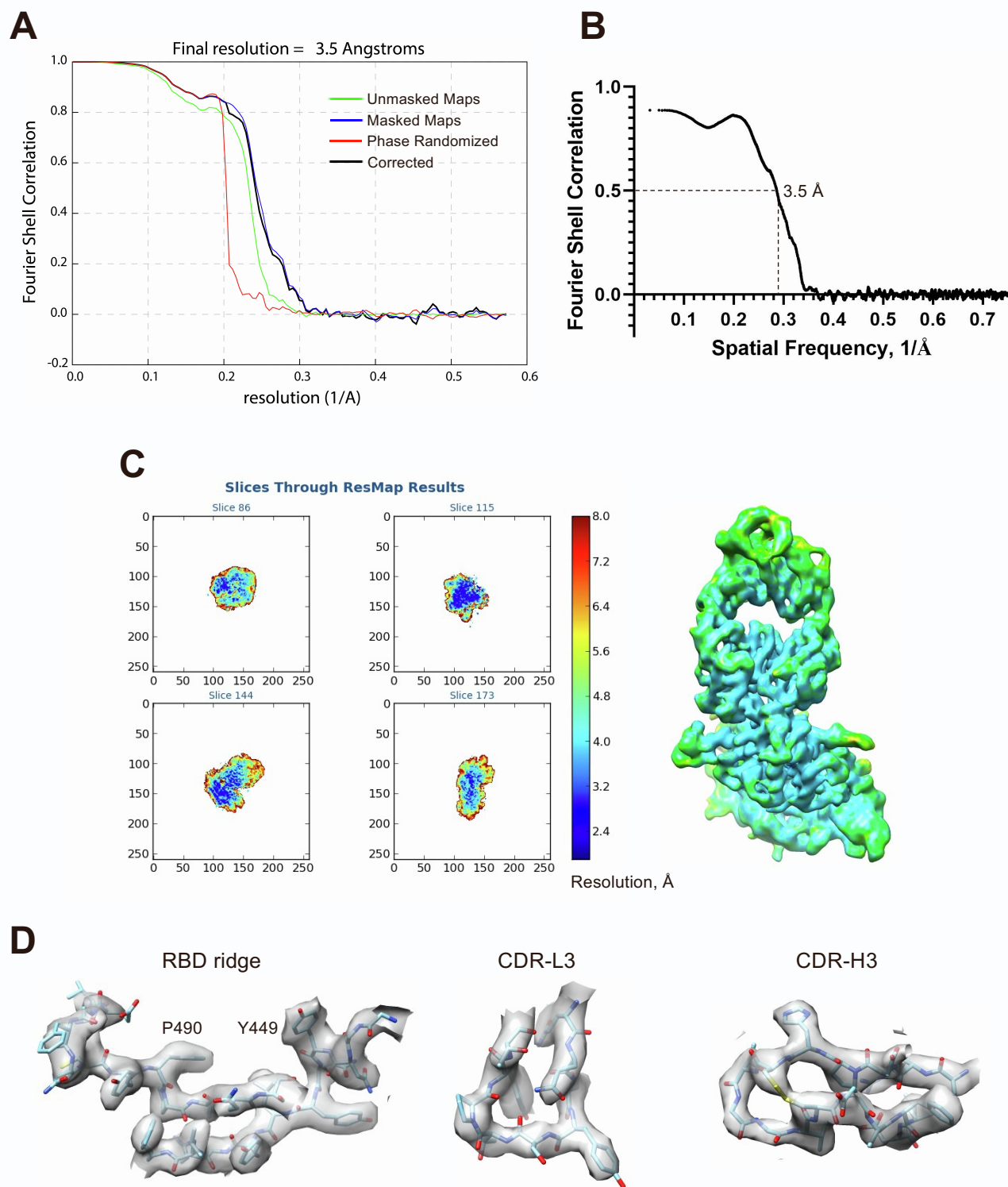(C) Local resolution determined with ResMap.
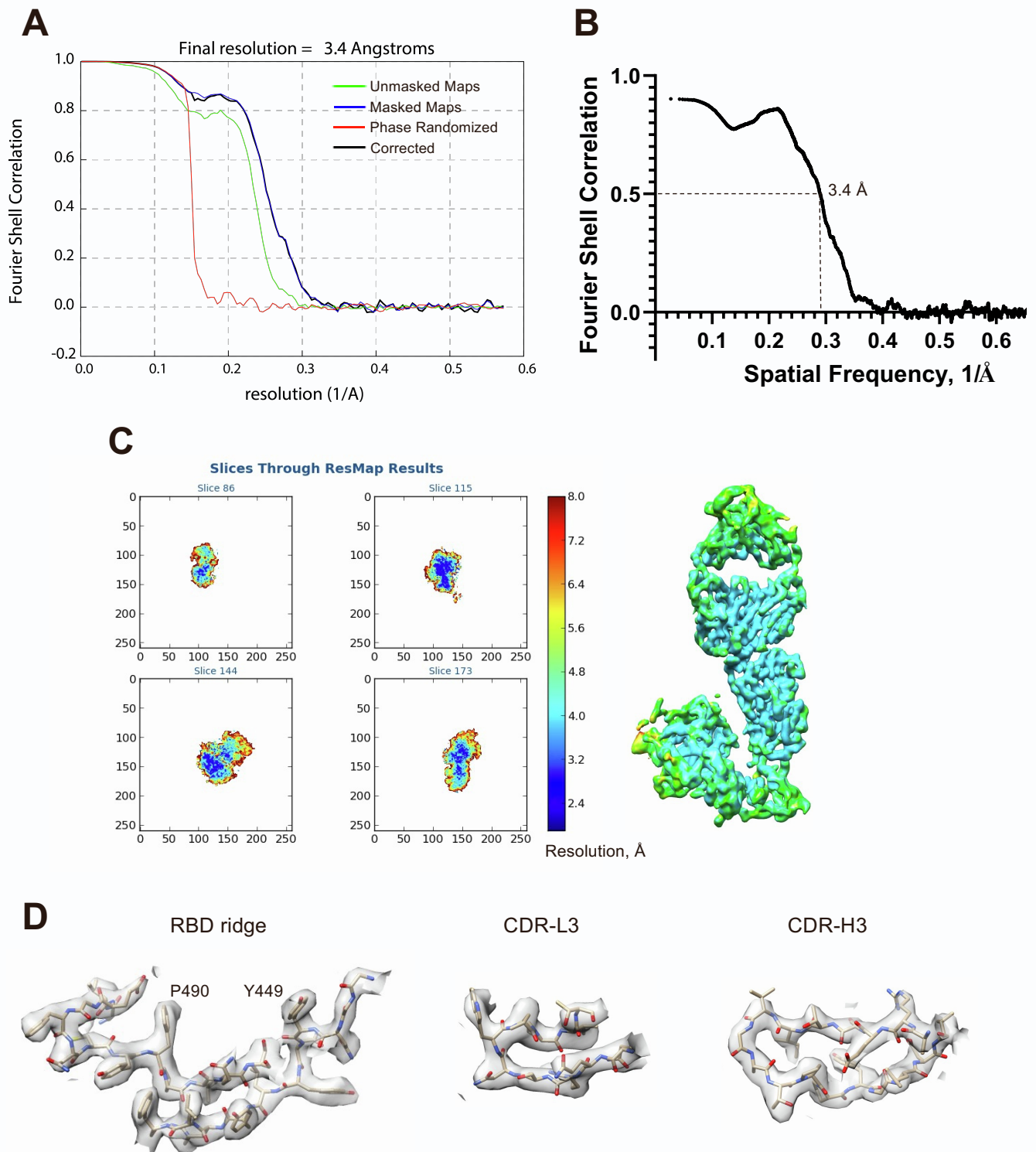
Figure S10. Validation of the local cryo-EM structure of SARS-CoV-2 receptor binding domain (RBD) in complex with Fab NE12, related to Figure 3.

(A) Fourier shell correlation (FSC) plots generated by Relion.

(B) FSC curve between the map and atomic model.

(C) Local resolution determined with ResMap.
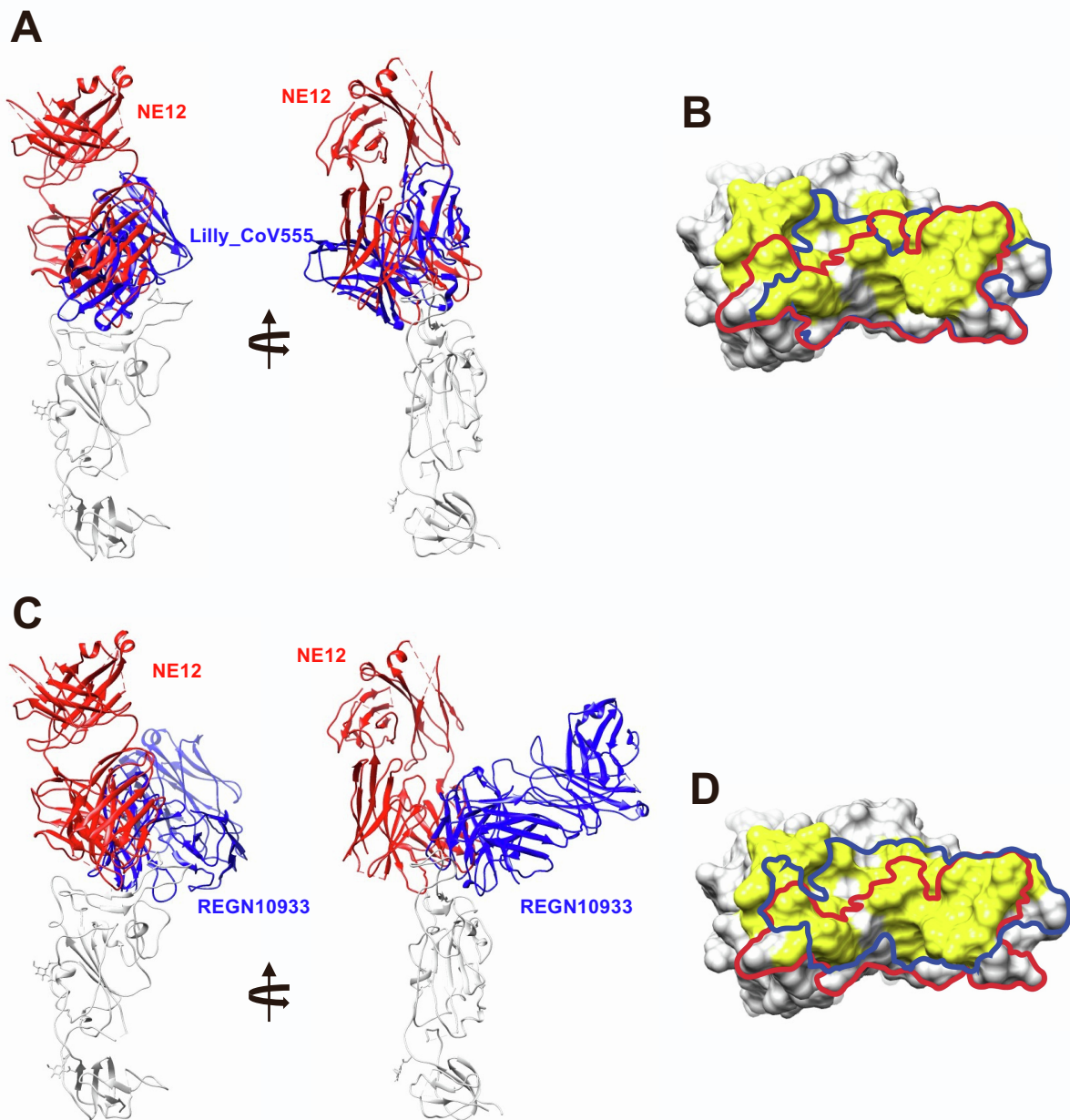
(D) Examples of cryo-EM density.

Figure S11. Validation of the local cryo-EM structure of SARS-CoV-2 receptor binding domain in complex with Fab NA8, related to Figure 4.

(A) Fourier shell correlation (FSC) plots generated by Relion.

(B) FSC curve between the map and atomic model.

(C) Local resolution determined with ResMap.

(D) Examples of cryo-EM density.

Figure S12. Comparison of binding modes and epitopes of RBD-directed antibodies NE12, Lilly_CoV555 and REGN10933, related to Figure 5.

(A) Cartoon representations of aligned RBD-Fab complexes for NE12 and Lilly_CoV555 (from PDB 7l3n).

(B) The RBD is shown in surface representation with the epitopes of NE12 and Lilly_CoV555 outlined with red and blue curves, respectively. Surface areas corresponding to the RBD residues forming the ACE-2 receptor interface are colored yellow.

(C) Cartoon representations of aligned RBD-Fab complexes for NE12 and REGN10933 (from PDB 6xdg).

(D) The RBD is shown in surface representation with the epitopes of NE12 and REGN10933 outlined with red and blue curves, respectively. Surface areas corresponding to the RBD residues forming the ACE-2 receptor interface are colored in yellow.
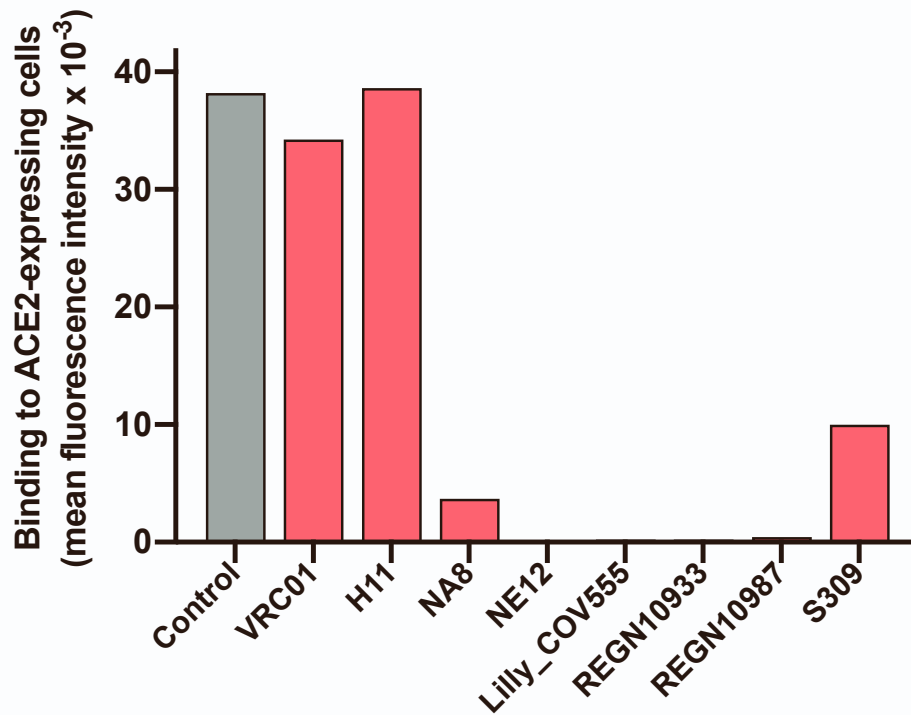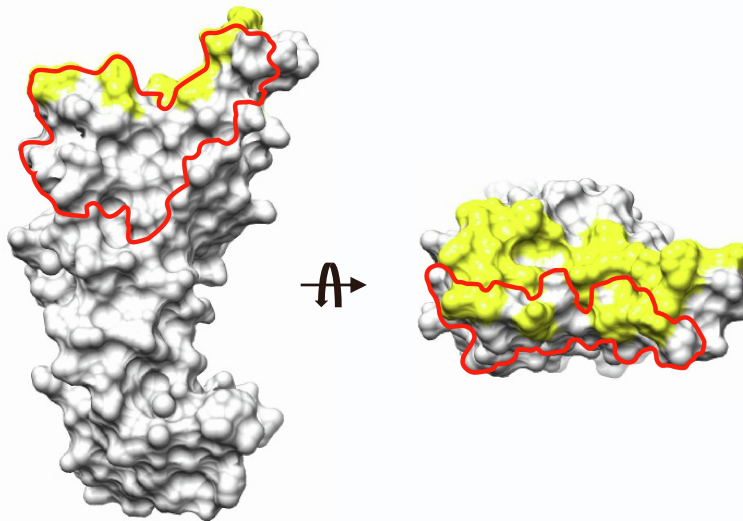
Figure S13. Competition of various mAbs with S-6P trimer binding to ACE-2-positive cells, related to Figure 5.

(A) Ability of monoclonal antibodies against the SARS-CoV-2 spike to block the interaction of the S-6P trimer to ACE2-expressing HEK293 cells. The trimer was directly labeled with phycoerythrin (PE) and pre-incubated with each of the mAbs or with PBS buffer (control) for 30 min before incubation with the cells for 30 min.

(B) Overlap between the NA8 epitope and the ACE2 footprint. The RBD is shown in surface representation. The epitope of NA8 is outlined with a red line. The ACE2 interface is colored in yellow.
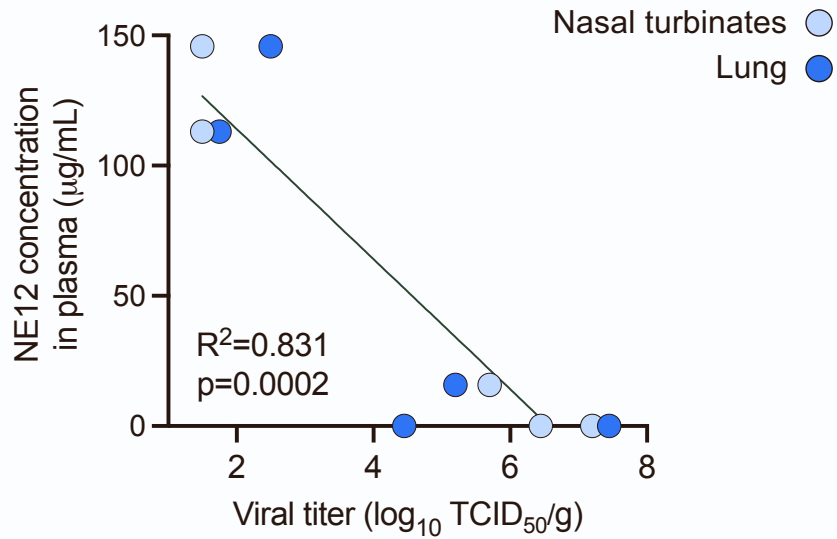
Figure S14. Plasma concentrations of anti-SARS-CoV-2 spike human antibodies in hamsters treated with mAbs NE12 and NA8, related to Figure 7. Mean plasma levels of NE12 and NA8 in hamsters treated with the mAbs 24 hours after virus challenge with the original strain, WA-1, or the B.1.351 variant. The mAb concentrations were determined using a specific ELISA with the recombinant S-protein trimer (S-2P) immobilized on the plastic surface. The data represent mean values from 5 animals (± SEM).

Table S1. Demographic characteristics and neutralizing antibody titers in 12 COVID-19 convalescent plasma donors, related to Figure 1

Patient number	1	2	3	4	5	6	7	8	9	10	11	12
Age	65	60	53	35	49	40	66	62	58	52	54	61
Gender	F	F	M	M	M	M	F	M	F	F	M	F
Neutralizing antibody titer	80	80	80	80	320	320	320	160	160	640	160	640
Blood collected (mL)	40	35	19	24	24	40	22	28	38	40	32	18

Table S2. Binding affinity of anti-SARS-CoV-2 Fabs to the S-2P trimer, as measured by surface plasmon resonance, related to Figure 1

Fab	K_D (M)	k_d (s^{-1})	k_a (1/Ms)
1G8	6.2e-10	2.0e-4	4.6e5
3F6	4.3e-10	8.2e-4	3.9e6
4B6	8.7e-10	1.1e-3	1.3e6
D12	7.2e-10	8.7e-4	1.3e6
NA8	4.6 e-10	1.2e-3	2.8e6
2A12	3.0e-10	8.0e-4	2.7e6
NE8	1.8e-10	5.7e-3	3.1e6
NE12	6.1e-10*	6.5e-4	1.3e6
NG3	2.2e-10	2.0e-4	1.0e6
4B7	1.1e-9	1.7e-3	1.6e6
A7	3.9e-10	7.8e-4	2.2e6
H11	6.5e-9	1.7e-3	2.7e5

*Constants were determined using BiaEvaluation software. Constants are the average of two different analyses. Only one reliable data set was obtained for 4B7.

Table S3. Genetic properties of 18 Fabs specific for the spike (S) protein of SARS-CoV-2, related to Figure 1

Fab	Heavy chain						Light chain				
	VH	JH	DH	HCDR3	CDR3 length	VH SHM	VL	JL	LCDR3	CDR3 length	VL SHM
G6	1-24	5	6-13	CATAPAIAAAYTGWFDPW	16	4	LV2-14	LJ2	CSSYAGSSVVF	9	9
4A12	3-9	6	2-15	CVRGEILGDDYYRMDVW	15	14	KV1-39	KJ4	CQQSYSTPLTF	9	0
4B7	3-30-3	4	1-26	CARPHSGSYFSHFDYW	14	8	KV3-20	KJ1	CQQYGSSPWTF	9	0
A7	1-69	6	3-10	CANGAHNWGSGFSYYYSYMDVW	20	5	KV3-20	KJ4	CQQYGSSPLTF	9	0
1B1	1-69	6	4-17	CARYIPDFGDYVTPYYYYALDVW	21	15	KV1-39	KJ4	CQQSYSTPLTF	9	0
4C6	3-30	3	4-23	CARSYGGNYLSAFDVW	14	11	KV3-15	KJ3	CQQNNEWPLTF	9	9
H11	1-46	3	3-10	CVYDTGPHAFDIW	11	3	LV1-51	LJ3	CGTWDSSLSVWVF	11	2
1G8	1-2	6	D1-7	CARDRKFDSNWNYDKGRYGMDVW	21	12	KV1-39	KJ4	CQQSYTLTF	7	6
3F6	1-2	4	3-22	CARVPRNYYDRRGSLVYEDYFEYW	22	8	KV3-20	KJ2	CQQFGSPPITF	9	6
3B6	3-23	4	3-22	CAKVGRRSNTLIVVATEFDYW	19	14	KV1-39	KJ3	CQQGYSTPPLFTF	11	6
4B6	1-69	6	4-11	CARDSTESPLYGMDVW	14	8	KV1-39	KJ2	CQQSYSTPLTF	9	0
D12	3-13	3	3-16	CARGGPLGGGEDAFDMW	15	9	KV1-5	KJ2	CQHYSGYPYTF	9	16
NA8	3-33	3	2-8	CARDPHCTGGVCDAFDLW	16	15	KV1-39	KJ2	CQQSYSTPYTF	9	1
2A12	1-2	4	3-22	CARTLYYYDSSGNLSLDHW	17	7	KV1-39	KJ3	CQQSYSSQWTF	9	24
NE8	1-69	4	2-15	CARGHRYCSGGSCFPYFDYW	18	5	KV1-39	KJ2	CQQSYSTPRTF	9	0
NE12	1-2	6	1-26	CAREETIVGATPPYGLDVW	17	6	KV3-11	KJ5	CQQRSNWPPVTF	10	1
NF8	1-69	4	3-16	CAGVEAYHDSIWGTFAPRYYFGSW	22	14	KV1-39	KJ3	CQQSYSSPPTF	9	0
NG3	1-69	4	5-18	CARVSGYSFGPYFDYW	14	6	KV3-11	KJ3	CQQRSSWPPTF	9	0

Table S4. Cryo-EM data collection and analysis statistics, related to Figures 3 and 4

	S-6P in complex with Fab NE12		S-6P in complex with Fab NA8	
Data collection and processing				
Magnification	105,000		105,000	
Voltage (kV)	300		300	
Electron exposure (e⁻/Å²)	40		40	
Defocus range (μm)	-1.0 to -2.5		-1.0 to -2.5	
Pixel size (Å)	0.873		0.873	
Symmetry imposed	C1		C1	
Initial particle images (no.)	2,253,882		2,870,476	
Final particle images (no.)	201,607		454,910	
	Consensus map EMDB-26401	Local map EMDB-26402 PDB 7U9O	Consensus map EMDB-26403	Local map EMDB-26404 PDB 7U9P
Map resolution (Å)	3.1	3.4	2.9	3.5
FSC threshold	0.143		0.143	
Map resolution range (Å)	1.9-6.8	3.1-6.8	1.9-8.0	3.1-6.8
Refinement				
Initial model used (PDB code)		6xlu		6xlu
Model resolution (Å)		3.4		3.5
FSC threshold		0.5		0.5
Map sharpening *B* factor (Å²)	-44.4	-125.7	-53.3	-165.1
Model composition				
Non-hydrogen atoms		6563		6126
Protein residues		829		777
Ligands (glycans)		3		4
Water		0		0
B factors (Å²) (mean)				
Protein		58.9		65.8
Ligand		82.1		103.7
Water		N/A		N/A
R.m.s. deviations				
Bond lengths (Å)		0.007		0.013
Bond angles (°)		0.926		1.19
Validation				
MolProbity score		1.44		1.63
Clash score		1.55		2.49
Poor rotamers (%)		0.28		0.15
Ramachandran plot				
Favored (%)		90.34		88.16
Allowed (%)		9.53		11.57
Disallowed (%)		0.13		0.27